Journal of Computational Applied Mechanics 2024, 55(-): PP-PP
DOI: 10.22059/JCAMECH.2024.374727.1029

RESEARCH PAPER

An investigation into the numerical analysis of refined higher order shear deformation theory for frequency responses of two-directional functionally graded taper beams.

G. Chandra Mohana Reddy [a, *], Ch Ravikiran [a], S Nagaraju [a], P. Bridjesh [b]

[a] *Department of Mechanical Engineering, MLR Institute of Technology, Hyderabad, India*
[b] *Department of Chemical & Materials Engineering, College of Science, Engineering and Technology, University of South Africa (UNISA), c/o Christiaan de Wet & Pioneer Avenue, Florida Campus 1710, Johannesburg, South Africa*

Abstract

For the aircraft and space shuttles to have the right properties, they need new engineering materials. Changing the qualities of the material in more than one direction is one way to do this. These features should be seen in in-plane, bi-directional functionally graded materials. This study examines the vibration behavior of a two-directional functionally graded taper beam (TDFGTB) with uniform load distribution. The analysis uses a refined higher-order shear deformation theory**, Lagrange equations, and the displacement functions are formulated in simple algebraic polynomials incorporating admissible functions to satisfy the boundary conditions in both directions with the help of a Ritz-type solution. The components of admissible functions are derived from Pascal's triangle. The study also examines the influence of taper ratios, aspect ratios, and gradation exponents on the vibration response. The results provide a benchmark for assessing beam theories and are crucial for optimizing the design of TDFGTBs.**

Keywords : Refined Higher-order Shear Deformation Theory, Two-Directional Functionally Graded Taper Beam, Hamilton's principle, Ritz type solution, Frequency responses.

1. Introduction

An essential aspect of developing structural design and guaranteeing structural integrity is the examination of the vibration properties of Two-directional Functionally Graded Taper Beam (TDFGTB) using refined higher-order shear deformation theory (RHSDT). Understanding of the dynamic characteristics exhibited by Functionally Graded Materials (FGM) within tapered beam structures facilitates the enhancement of material gradients and leads to progress in various engineering domains such as heat shields in aircraft, fusion reactors, heat exchangers, turbine blades, etc. in which the material experiences a significantly elevated temperature field characterized by a substantial temperature gradient both on the surface and inside its thickness [1].

Intricate structural components encounter dynamic loads that result in vibration. In some instances, the magnitude of dynamic loading might be sufficiently intense to result in significant deformations, hence introducing complexity to the system via the induction of geometric nonlinearity. FGMs have attracted considerable interest in the structural engineering field owing to their distinctive characteristics, which exhibit continuous variation throughout their volume [2]. Stress concentrations in homogeneous materials may cause early failure under specific loading circumstances, while FGMs may improve load-bearing and stress distribution by gradually changing their material composition.

Previous research has examined many aspects of vibration analysis in functionally graded taper beams (FGTB), providing significant contributions to understand their dynamic characteristics and structural performance. conducted a comparative analysis on the effectiveness of 1D and 3D models in modeling free vibrations of FGTBs using ABAQUS and found that as FGTB geometric complexity and material inhomogeneity increase, the differences between models become more noticeable [3]. conducted a comparative analysis of deflections in a FGTB under a uniformly distributed load using the higher-order shear deformation theory (HSDT), power-law formula, Hamilton's principle, and Navier's solutions and concluded that the geometrical factors influence the structural analysis of the beam [4]. used HSDT and von-Kármán's nonlinear geometric relation to create linear and nonlinear isogeometric finite element models for an FGTB with graphene platelet-reinforced composite and the nonlinear bending and

* Corresponding author. Tel.: +91-8297909752; fax: +0-000-000-0000 .
E-mail address: cmreddy115@gmail.com

vibration responses were examined through parametric studies [5]. Explored the relationship between size and nonlinear free longitudinal vibration of axially functionally graded nanorods using nonlocal elasticity theory while using Hamilton's principle to compute nonlinear natural frequencies [6].

conducted a numerical study on dimensionless natural frequencies of non-uniform aluminum beams covered with FGM and found that the width of the beams exhibits variability, coating material's characteristics change according to a polynomial function and highlighted the importance of considering the critical threshold for shape variation [7]. investigated the vibrations of a cantilevered conical beam, focusing on the non-linear impacts of curvature and inertia on the frequency response using the Euler-Bernoulli beam theory and Hamiltonian mechanics principles and explored the influence of material distribution on the system's frequency response during the early resonance stage, integrating finite gradient methodology and nonlinear dynamics [8]. studied the vibration mechanics of a porous bi-directional functionally graded doubly curved sandwich shell using HSDT theory and the p-version finite element technique and explored the impact of gradient indices and porosity distribution on performance [9]. conducted a nonlinear study on a cantilever bar element made of graded material with porosity characteristics, considering the axial orientation, material properties, and stress-strain relationship and found that porosity and material graduation significantly influenced the bar element's nonlinear behavior [10, 11]. They developed a closed-form solution for frequency vibration, incorporating nonlocal parameters in Bessel functions and found that in-plane pre-loads significantly influence natural frequencies for decreasing radii of the circular nanoplate [12].

Various solution methods have been proposed for solving the governing equations that assess the vibration of Functionally Graded Beams (FGB). The primary objective of analytical approaches is to get precise solutions to the differential equations, considering simplifying assumptions and using closed-form solutions such as exact solutions as adapted by, typically based on Galerkin and state space formulation [13]. The method of initial values was adapted by to consider the small-scale effects occurring in structures of smaller size [14]. Solved the governing equation of motion for vibration analysis using the Galerkin method and parametric investigations have been conducted on elastic foundations to examine the outcomes and applicability to real-world issues and concluded that the varied foundation exerts a substantial impact on the FGM [15]. Studied the nonlinear behavior of a porous functionally graded Euler-Bernoulli nanobeam under mechanical and electrical loads using nonlocal strain gradient elasticity theory. They used Hamilton's principle, Galerkin techniques and other methods to solve governing equations for various boundary conditions. The findings revealed that length-scale characteristics significantly influence the nonlinear vibration behavior of these devices [16].

Conducted a study on the free vibration analysis of FGTB to observe the impact of shear strain and solved the governing equations using the complementary functions method [17]. proposed the generalized differential quadrature method (GDQM) for solving the governing equation and estimating the coefficients for assessing the structural mechanics of a Timoshenko nanobeam which is functionally graded and tapered [18]. GDQM was also used by in assessing the vibration analysis of a FGTB composed of piezoelectric material [19]. The isogeometric analysis was adapted by in studying the vibration characteristics of curved microbeams. Utilizing numerical approaches, the beam domain is discretized using numerical methods, and the governing equations are solved by utilizing numerical methods [20]. used Fredholm integral equations to analyze the free vibration in a FGTB and studied the effect of axial force and shear deformation [21]. studied nanocomposite microbeams reinforced with FGTB, focusing on size-dependent free vibration and buckling characteristics and suggested that synchronized axial distributions could enhance buckling resistance and natural frequency, while used homogenization methodology to assess microbeam vibration mechanics [22, 23]. Studied thermal-induced shear buckling of orthotropic single-layered graphene sheets using nonlocal elasticity theory and the differential quadrature method. They analyzed six border conditions, considering elastic media, temperature variations, material properties, and boundary conditions [24].

Used the Chebyshev-Ritz method to compute buckling and compared it with buckling tests on composites made from epoxy resin, glass fiber, and nanorods and found that nanorods enhance tensile strength, rigidity, and critical buckling load [25]. Studied a sandwich composite beam strengthened with carbon nanorods from potato waste that was subjected to axially variable force, and the behavior of the beam was analyzed using strain gradient, general strain theory, shear deformation theory and HSDT. They found that using recycled materials enhances sandwich beam rigidity and increase critical buckling loads [26]. Examined the stability of a spinning viscoelastic sandwich beam with a soft core and carbon nanotube reinforced metal matrix nanocomposites skin, focusing on residual stress effects and the governing equations of motion for a rotating viscoelastic sandwich beam. Factors such as carbon nanotube distribution, volume fraction, spinning speed, critical loading, core thickness, axial force, and residual stress were investigated and suggested that varying spinning speeds can determine the ideal core thickness to prevent instability [27]. Studied the vibration characteristics of multilayered piezoelectric nanobeams using Timoshenko beam theory, nonlocal continuum theory, surface elasticity theory and the differential quadrature method [28]. Studied the vibration behaviors of a micro-cylindrical sandwich panel using carbon nanotubes and graphene platelets as renforcements with porous and foam cores and analyzed higher-order shear deformation theory. They found that natural frequencies decrease with temperature but increase with SMA materials. The impact of different core materials on sandwich composite plates' low velocity impact behavior, to design and manufacture samples with more stored energy against impact and to find light sandwich structures [29]. The method for synthesizing hollow magnetic spheres with antibacterial properties, which could be useful in medicine, particularly cancer treatment and a hydrothermal method for synthesizing carbon nano-arrays using locally available materials using stainless steel type 1.4401 for autoclave system construction [30, 31].

Studied the oscillation characteristics of a sandwich beam with a porous core and composite face layers with shape memory alloy (SMA) under free and forced vibrations. They used Vlasov's model, Hamilton's principle, first-order shear deformation theory, Navier's method and validated results using relevant literature sources, while the key variables included temperature, SMA volume fraction, porosity distribution, CNT weight fraction, and geometric factors [32, 33]. Analyzed the structural properties of

a sandwich beam strengthened with carbon nanotubes/graphene origami auxetic metamaterials (GOAM) and porous cores. They used the variational iteration method (VIM) to solve the equations of motion under different boundary conditions. Factors such as carbon nanotube distribution, porosity coefficient, porous core type, porosity parameter, weight fraction, and GOAM folding degree were examined. The results showed a strong agreement with previous studies, with a maximum error percentage of 0.3% for the first five frequencies and 0.22% for the first frequency [34, 35]. The buckling, vibration and deflecitons in a five-layer sandwich nanocomposite beam, with reinforcements of graphene platelets (GPLs) and shape memory alloys (SMAs), and a foam core was investigated and the Coriolis effect on the vibration analysis was investigated [36, 37]. Studied the oscillation characteristics of circular graphene sheets under in-plane pre-load.

Prior studies on vibration analysis in FGBs have made significant contributions to the comprehension of their dynamic properties and structural applicability. The findings of a comparative study indicate that there is an increasing variation in the geometric complexity along with material inhomogeneity of FGBs. Research has also investigated the deflections in FGBs when subjected to homogenous loads, with a focus on the impact of geometrical parameters on structural analysis. The assessment of FGB vibrations has been conducted using various kinds of solution techniques, including analytical, semi-analytical, and numerical approaches.

This research paper highlights a significant gap in existing literature, highlighting a lack of comprehensive exploration of free vibration characteristics in TDFGTBs using RHSDT. This study aims to create a model of a TDFGTB, extract the governing equation that describes the vibration characteristics of the TDFGTB. This will be done by employing the displacement fields and stress-strain relations, which are based on Hooke's law. The solution to the governing equation will be achieved using the Ritz technique. The accuracy of the developed beam model is confirmed by comparing it with existing data in scientific literature, and further verified by considering both alumina and aluminum as potential materials for the beam to thoroughly investigate the behavior of free vibration in TDFGTB, adapting RHSDT under different boundary conditions. Vibration analysis of TDFGTB using RHSDT is essential for understanding the dynamic behavior of functionally graded taper beams, facilitating their design, analysis, and optimization in various engineering applications such as aerospace, automotive, civil structures, and biomedical devices.

2. Nomenclature

x, y, z	Different coordinates along length, width, thickness directions of beam
TD	Two dimensional
FGB	Functionally graded beam
SS	Simply supported
CC	Clamped-clamped
L	Length
K	Kinetic energy
h	Height
Vf	Volume fraction
Pz	Gradient index in thickness direction
Px	Gradient index in length direction
F(z)	Shear shape function
HSDT	Higher order shear deformation theory
E	Modulus of elasticity
μ	Poisson's ratio
ρ	Mass density α coefficient of porosity
f(z)	Shear shape function σx Axial stress τxz Shear stress
RHSDT	Refined higher-order shear deformation theory
U	Strain energy
c	Ceramic
m	Metal
n	Taperness parameter
TBT	Timoshenko beam theory

3. Material properties of TDFGTB

The study favors TDFGTBs due to their variation in composition, material parameters, and thickness. The non-uniform beams have h_2 and h_1 thicknesses, determined by the equation $h(x) = h_2 [1 - n(x/L)]$. The prevailing view is based on fundamental assumptions.

- In accordance with the Cartesian coordinate system, the point of origin is situated on the neutral surface of the FG beam.
- In comparison to the transverse normal stress, σ_z, the normal stress in the plane, σ_x, is virtually insignificant.
- In order to satisfy the criteria for the lower and upper beam boundaries, this theory requires the application of a shear correction factor and operates under the supposition of a constant transverse shear stress.

RHSDT is adopted in this study as it includes higher-order terms in the displacement field compared to conventional theories. These additional terms account for effects like transverse shear deformation and thickness stretching, which are significant in thin structures but are neglected in simpler theories.

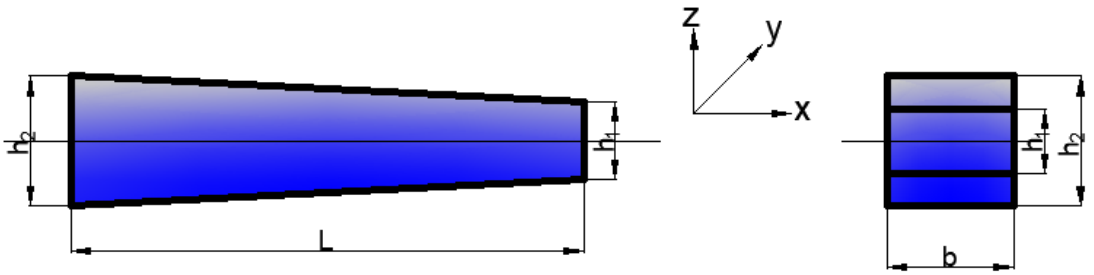

Fig 1 : Geometry of FG Taper Beam.

Fluctuations in the volume proportion of the component materials cause TDFGTB properties to constantly fluctuate. Let's consider a functional correlation between the thickness coordinate and certain material properties. The volume fraction of metal (V_m) can be mathematically represented using the power law equation [16].

$$V_f(x,z) = \left(\frac{x}{L}\right)^{px}\left(\frac{1}{2}+\frac{z}{h(x)}\right)^{pz} \quad (1)$$

TDFGTB's material characteristics are as follows [16] :

$$P(x,z) = (P_c - P_m)\left(\frac{x}{L}\right)^{px}\left(\frac{z}{h(x)}+\frac{1}{2}\right)^{pz} + P_m \quad (2)$$

'*m*' stands for metal phase and '*c*' for ceramic phases. 'Px' and 'Pz' denote power law exponents. As illustrated in Fig 2, the power law exponents are ($P_x = P_z$ = 0, 0.1, 0.2, 0.3, 0.4, 0.5, 0.6, 0.7, 0.8, 0.9, 1).

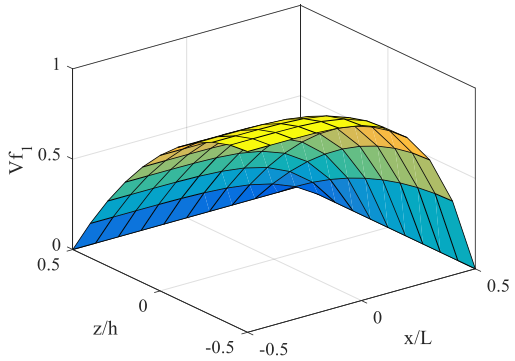

Fig 2 : Metal volume fractions in the direction of length (x/L) and thickness (z/h).

3.1. TDFGTB Formula

The following is a list of the TDFGTB's density ("ρ"), Poisson's ratio ("μ"), and modulus of elasticity ("E") [16].

$$E(x,z) = (E_c - E_m)\left(\frac{z}{h(x)}+\frac{1}{2}\right)^{pz}\left(\frac{x}{L}\right)^{px} + E_m \quad (3)$$

$$\rho(x,z) = (\rho_c - \rho_m)\left(\frac{z}{h(x)}+\frac{1}{2}\right)^{pz}\left(\frac{x}{L}\right)^{px} + \rho_m \quad (4)$$

3.2. Constitutive equations of displacement

RHSDT with a shear strain function is considered in order to illustrate the displacement equations [2].

$$u(x,z,t) = u_0(x,t) - z\frac{\partial w_0}{\partial x}(x,t) + f(z)\phi(x,t) \quad (5)$$

$$w(x,z,t) = w_0(x,t) \quad (6)$$

u_0, w_0, and $\frac{dw_0}{dx}$ indicate axial displacement, transverse displacement, and shear slope at a given position on a neutral axis. The displacement fields offer a versatile foundation for representing intricate deformations in structures. By decomposing the displacement into primary and additional components, the beam model is able to accommodate different loading situations and boundary conditions, resulting in a more precise depiction of the structural response. The additional displacement term $f(z)\phi(x,t)$ allows for the incorporation of any other applied loads or boundary conditions that may affect the structural response. This flexibility enables the model to capture a wide range of loading scenarios, including external forces, thermal effects, or constraints imposed by the surrounding environnement. Utilizing the inverse elastoplastic function, or shear shape function, *f(z)* [2], to calculate the transverse shear deformation distribution.

$$\varepsilon_x = \frac{\partial U}{\partial x} = \frac{\partial u_0}{\partial x} - z\frac{\partial^2 w_0}{\partial x^2} + f(z)\left(\frac{\partial \phi}{\partial x}\right) \quad (7)$$

$$\varepsilon_z = \frac{\partial w}{\partial z} = 0 \quad (8)$$

$$\gamma_{xz} = f'(z)\emptyset \quad (9)$$

$$f(z) = z\left[1 - \frac{4}{3}\left(\frac{z}{h}\right)^2\right] \quad (10)$$

$$f'(z) = \left[1 - 4\left(\frac{z}{h}\right)^2\right] \quad (11)$$

where,
ε_x is strain in x-direction
ε_z= strain in z-direciton
γ_{xz}= shear strain
As Hooke's rule is always obeyed by the beam in FGMs, the behavioural relations may be expressed in the following format :

$$\begin{Bmatrix}\sigma_x\\ \tau_{xz}\end{Bmatrix}=\begin{bmatrix}Q_{11}(z) & 0\\ 0 & Q_{55}(z)\end{bmatrix}\begin{Bmatrix}\varepsilon_x\\ \gamma_{xz}\end{Bmatrix} \quad (12)$$

$$Q_{11}(\mathrm{z})=\frac{E(x,z)}{1-\mu^2} \quad (13)$$

$$Q_{55}(z)=\frac{E(x,z)}{2(1+\mu)} \quad (14)$$

3.3. Motion-Governing Equations

From Hamiltonian principle the equations of motion are derived and can be expressed as follows in the time span [0, t]:

$$\int_0^T \delta(U-K)\,dt=0 \quad (15)$$

Where δk denotes the fluctuation of kinetic energy and δU denotes the variation of strain energy [4].

Strain Energy, $U=\frac{1}{2}\,\sigma\ \varepsilon\ V$ (16)

Kinetic Energy, $K=\frac{1}{2}\ m\ V^2$

$$=\frac{1}{2}\ \rho\ v\ V^2 \quad (17)$$

3.4. Formulation of free vibration

Bi-directional functionally graded beam's strain energy can be expressed as [4] :

$$U=\frac{1}{2}\int_0^L\int_{-\frac{h}{2}}^{+\frac{h}{2}}(\sigma_x\varepsilon_x\ +\tau_{xz}\gamma_{xz})dzdx \quad (18)$$

Equations (8), (10), (13), and (14), respectively, are substituted into Equation (18), the strain energy can be expressed as,

$$U=\frac{1}{2}\int_0^L\int_{-\frac{h}{2}}^{+\frac{h}{2}}\left(\frac{E(x,z)}{1-\mu^2}\varepsilon_x\varepsilon_x\ +\frac{E(x,z)}{2(1+\mu)}\gamma_{xz}\gamma_{xz}\right)dzdx \quad (19)$$

$$\mathrm{U}=\frac{1}{2}\int_0^{\mathrm{L}}\int_{-\frac{\mathrm{h}}{2}}^{+\frac{\mathrm{h}}{2}}\left[\left(\frac{\mathrm{E(x,z)}}{1-\mu^2}\left(\left(\frac{\partial \mathrm{u_0}}{\partial \mathrm{x}}\right)^2-2\mathrm{z}\frac{\partial \mathrm{u_0}}{\partial \mathrm{x}}\frac{\mathrm{d^2w_0}}{\mathrm{dx^2}}+2\,\mathrm{f(z)}\frac{\partial \mathrm{u_0}}{\partial \mathrm{x}}\frac{\partial \emptyset}{\partial \mathrm{x}}+\mathrm{z}^2\left(\frac{\mathrm{d^2w_0}}{\mathrm{dx^2}}\right)^2-2\,\mathrm{f(z)}\frac{\mathrm{d^2w_0}}{\mathrm{dx^2}}\frac{\partial \emptyset}{\partial \mathrm{x}}+(\mathrm{f(z)})^2\left(\frac{\partial \emptyset}{\partial \mathrm{x}}\right)^2\right)\right)+$$

$$\frac{\mathrm{E(x,z)}}{2(1+\mu)}(\emptyset^2(\mathrm{f'(z)})^2)\Bigg]dzdx \quad (20)$$

The kinetic energy of TDFGTB can be written in similar way :

$$K=\frac{1}{2}\int_0^L\int_{-\frac{h}{2}}^{+\frac{h}{2}}\left[\left(\rho(z)\left(\left(\frac{\partial u_0}{\partial t}\right)^2-2\mathrm{z}\frac{\partial u_0}{\partial t}\frac{d^2w_0}{dxdt}+2\,\mathrm{f(z)}\frac{\partial u_0}{\partial t}\frac{\partial \phi}{\partial t}+z^2\left(\frac{d^2w_0}{dxdt}\right)^2-2\,\mathrm{f(z)}\frac{d^2w_0}{dxdt}\frac{\partial \phi}{\partial t}+(\mathrm{f(z)})^2\left(\frac{\partial \phi}{\partial t}\right)^2\right)\right)+$$

$$\frac{E(\mathrm{x,z})}{2(1+\mu)}(\phi^2(\mathrm{f'(z)})^2)\Bigg]dzdx \quad (21)$$

The displacement functions display the kinematic boundary conditions, which are represented in terms of generalized coordinators and expressed in infinity dimensions in Lagrange equations derived from Hamilton's principle [4].

$$\mathrm{u(x,t)}=\sum_{\mathrm{j=1}}^{\mathrm{m}}\mathrm{A_j}\theta_\mathrm{j}(\mathrm{x})\mathrm{e}^{\mathrm{i}\omega\mathrm{t}},\quad \theta_j(x)=\left(x+\frac{L}{2}\right)^{p_u}\left(x-\frac{L}{2}\right)^{q_u}x^{m-1} \quad (22)$$

$$w(x,t)=\sum_{j=1}^{m}B_j\varphi_j(x)e^{i\omega t},\quad \varphi_j(x)=\left(x+\frac{L}{2}\right)^{p_w}\left(x-\frac{L}{2}\right)^{q_w}x^{m-1} \quad (23)$$

$$\phi(x,t)=\sum_{j=1}^{m}C_j\psi_j(x)e^{i\omega t},\quad \psi_j(x)=\left(x+\frac{L}{2}\right)^{p_\phi}\left(x-\frac{L}{2}\right)^{q_\phi}x^{m-1} \quad (24)$$

Boundary constraints for the proposed shape functions are $\theta_j(x)$, $\varphi_\mathrm{j}(x)$ and $\psi_\mathrm{j}(x)$.The complex numbers $i=\sqrt{-1}$ should be used to calculate the unknown coefficients A_j, B_j and C_j. By substituting the Equations. (22), (23) and (24) into (20) and (21) and then using Lagrange equations, deduced the governing equations of motion.

$$\frac{\partial \mathrm{U}}{\partial \mathrm{q_j}}+\frac{\partial}{\partial \mathrm{t}}\left(\frac{\partial \mathrm{k}}{\partial \dot{\mathrm{q}}_\mathrm{j}}\right)=0 \quad (25)$$

As a result of using q_j to represent the values of A_j, B_j and C_j,

$$\begin{bmatrix}[S_{11}] & [S_{12}] & [S_{13}]\\ [S_{12}]^T & [S_{22}] & [S_{23}]\\ [S_{13}]^T & [S_{23}]^T & [S_{33}]\end{bmatrix}-\omega^2\begin{bmatrix}[M_{11}] & [M_{12}] & [M_{13}]\\ [M_{12}]^T & [M_{22}] & [M_{23}]\\ [M_{13}]^T & [M_{23}]^T & [M_{33}]\end{bmatrix}\begin{Bmatrix}A\\ B\\ C\end{Bmatrix}=\begin{Bmatrix}\{0\}\\ \{0\}\\ \{0\}\end{Bmatrix} \quad (26)$$

The "stiffness" and "mass matrices" are denoted by [Ski] and [Mki], respectively. There must be symmetry and a maximum size for the stiffness and mass matrices. The stiffness and mass matrix's constituent parts are provided by,

$$S_{11}(i,j)=\int_{-L/2}^{L/2}\frac{E(x,z)}{1-\mu^2}\left[\left(x+\frac{L}{2}\right)^{p\theta}\left(x-\frac{L}{2}\right)^{q\theta}x^{i-1}\left(x+\frac{L}{2}\right)^{p\theta}\left(x-\frac{L}{2}\right)^{q\theta}x^{j-1}\right]dzdx \quad (27)$$

$$S_{12}(i,j)=-2\mathrm{z}\int_{-L/2}^{L/2}\frac{E(x,z)}{1-\mu^2}\left[\left(x+\frac{L}{2}\right)^{p\theta}\left(x-\frac{L}{2}\right)^{q\theta}x^{i-1}\left(x+\frac{L}{2}\right)^{p\varphi}\left(x-\frac{L}{2}\right)^{q\varphi}x,x^{j-1}\right]dzdx \quad (28)$$

$$S_{13}(i,j)=2f(z)\int_{-L/2}^{L/2}\frac{E(x,z)}{1-\mu^2}\left[\left(x+\frac{L}{2}\right)^{p\theta}\left(x-\frac{L}{2}\right)^{q\theta}x^{i-1}\left(x+\frac{L}{2}\right)^{p\psi}\left(x-\frac{L}{2}\right)^{q\psi}x^{j-1}\right]dzdx \quad (29)$$

$$S_{22}(i,j)=(z^2)\int_{-\frac{L}{2}}^{\frac{L}{2}}\frac{E(x,z)}{1-\mu^2}\left[\left(x+\frac{L}{2}\right)^{p\varphi}\left(x-\frac{L}{2}\right)^{q\varphi}x,x^{i-1}\left(x+\frac{L}{2}\right)^{p\varphi}\left(x-\frac{L}{2}\right)^{q\varphi}x,x^{j-1}\right]dzdx+(f(z))^2\int_{-\frac{L}{2}}^{\frac{L}{2}}\frac{E(x,z)}{2(1+\mu)}\left[\left(x+\frac{L}{2}\right)^{p\varphi}\left(x-\frac{L}{2}\right)^{q\varphi}x,x^{i-1}\left(x+\frac{L}{2}\right)^{p\varphi}\left(x-\frac{L}{2}\right)^{q\varphi}x,x^{j-1}\right]dzdx \quad (30)$$

$$S_{23}(i,j)=-(2f(z))\int_{-\frac{L}{2}}^{\frac{L}{2}}\frac{E(x,z)}{1-\mu^2}\left[\left(x+\frac{L}{2}\right)^{p\varphi}\left(x-\frac{L}{2}\right)^{q\varphi}x,x^{i-1}\left(x+\frac{L}{2}\right)^{p\psi}\left(x-\frac{L}{2}\right)^{q\psi}x^{j-1}\right]dzdx+(f(z))^2\int_{-\frac{L}{2}}^{\frac{L}{2}}\frac{E(x,z)}{2(1+\mu)}\left[\left(x+\frac{L}{2}\right)^{p\varphi}\left(x-\frac{L}{2}\right)^{q\varphi}x^{i-1}\left(x+\frac{L}{2}\right)^{p\psi}\left(x-\frac{L}{2}\right)^{q\psi}\right]dzdx \quad (31)$$

$$S_{33}(i,j)=(f(z))^2\int_{-\frac{L}{2}}^{\frac{L}{2}}\frac{E(x,z)}{1-\mu^2}\left[\left(x+\frac{L}{2}\right)^{p\psi}\left(x-\frac{L}{2}\right)^{q\psi}x^{i-1}\left(x+\frac{L}{2}\right)^{p\psi}\left(x-\frac{L}{2}\right)^{q\psi}x^{j-1}\right]+(f(z))^2\int_{-\frac{L}{2}}^{\frac{L}{2}}\frac{E(x,z)}{2(1+\mu)}\left[\left(x+\frac{L}{2}\right)^{p\psi}\left(x-\frac{L}{2}\right)^{q\psi}\left(x+\frac{L}{2}\right)^{p\psi}\left(x-\frac{L}{2}\right)^{q\psi}\right]dzdx \quad (32)$$

$$M_{11}(i,j)=\int_{-L/2}^{L/2}\rho(z)\left[\left(x+\frac{L}{2}\right)^{p\theta}\left(x-\frac{L}{2}\right)^{q\theta}x^{i-1}\left(x+\frac{L}{2}\right)^{p\theta}\left(x-\frac{L}{2}\right)^{q\theta}x^{j-1}\right]dzdx \quad (33)$$

$$M_{12}(i,j)=-(2z)\int_{-L/2}^{L/2}\rho(z)\left[\left(x+\frac{L}{2}\right)^{p\theta}\left(x-\frac{L}{2}\right)^{q\theta}x^{i-1}\left(x+\frac{L}{2}\right)^{p\varphi}\left(x-\frac{L}{2}\right)^{q\varphi}x,x^{j-1}\right]dzdx \quad (34)$$

$$M_{13}(i,j)=2f(z)\int_{-L/2}^{L/2}\rho(z)\left[\left(x+\frac{L}{2}\right)^{p\theta}\left(x-\frac{L}{2}\right)^{q\theta}x^{i-1}\left(x+\frac{L}{2}\right)^{p\psi}\left(x-\frac{L}{2}\right)^{q\psi}x^{j-1}\right]dzdx \quad (35)$$

$$M_{22}(i,j)=(z^2)\int_{-\frac{L}{2}}^{\frac{L}{2}}\rho(z)\left[\left(x+\frac{L}{2}\right)^{p\varphi}\left(x-\frac{L}{2}\right)^{q\varphi}x,x^{i-1}\left(x+\frac{L}{2}\right)^{p\varphi}\left(x-\frac{L}{2}\right)^{q\varphi}x,x^{j-1}\right]dzdx+(f(z))^2\int_{-\frac{L}{2}}^{\frac{L}{2}}\rho(z)\left[\left(x+\frac{L}{2}\right)^{p\varphi}\left(x-\frac{L}{2}\right)^{q\varphi}x,x^{i-1}\left(x+\frac{L}{2}\right)^{p\varphi}\left(x-\frac{L}{2}\right)^{q\varphi}x,x^{j-1}\right]dzdx \quad (36)$$

$$M_{23}(i,j)=-(2f(z))\int_{-\frac{L}{2}}^{\frac{L}{2}}\rho(z)\left[\left(x+\frac{L}{2}\right)^{p\varphi}\left(x-\frac{L}{2}\right)^{q\varphi}x,x^{i-1}\left(x+\frac{L}{2}\right)^{p\psi}\left(x-\frac{L}{2}\right)^{q\psi}x^{j-1}\right]dzdx+(f(z))^2\int_{-\frac{L}{2}}^{\frac{L}{2}}\rho(z)\left[\left(x+\frac{L}{2}\right)^{p\varphi}\left(x-\frac{L}{2}\right)^{q\varphi}x^{i-1}\left(x+\frac{L}{2}\right)^{p\psi}\left(x-\frac{L}{2}\right)^{q\psi}\right]dzdx \quad (37)$$

$$M_{33}(i,j)=(f(z))^2\int_{-\frac{L}{2}}^{\frac{L}{2}}\rho(z)\left[\left(x+\frac{L}{2}\right)^{p\psi}\left(x-\frac{L}{2}\right)^{q\psi}x^{i-1}\left(x+\frac{L}{2}\right)^{p\psi}\left(x-\frac{L}{2}\right)^{q\psi}x^{j-1}\right]+(f(z))^2\int_{-\frac{L}{2}}^{\frac{L}{2}}\rho(z)\left[\left(x+\frac{L}{2}\right)^{p\psi}\left(x-\frac{L}{2}\right)^{q\psi}\left(x+\frac{L}{2}\right)^{p\psi}\left(x-\frac{L}{2}\right)^{q\psi}\right]dzdx \quad (38)$$

4. Results and discussion

The factors that influence the vibration behaviour of TDFGTB are taper ratio, aspect ratio, gradation exponents and material property gradient. The taper ratio as well as the aspect ratio interact to establish the overall shape and distribution of stiffness in the beam. Increased taper ratios, when paired with decreased aspect ratios, yield more pronounced fluctuations in stiffness over the length of the beam. This, in turn, leads to the emergence of intricate vibration patterns and potentially higher frequencies of vibration modes. The gradation exponents determine the speed at which material qualities vary within the layers of FGMs. By including material property gradients, such as varying Young's modulus towards the outer surface of the beam, the stiffness profile and dynamic response of the beam are affected. When the gradation exponents are higher and there are steep gradients in material properties, the stiffness as well as mass distribution vary more significantly, resulting in noticeable differences in vibration characteristics. The numerical studies based on RHSDT shown in Table 1 are performed to predict the static analyses of TDFGTB with various boundary conditions, like SS and CC. Vibration analysis is discussed and shows that the existing hypothesis is accurate. Results constructed of "alumina" and "aluminium" with the following material properties are taken into account for the TDFGTB model :

Alumina : E_c=380 Gpa, $\rho_c = 3960\,\frac{\text{kg}}{\text{m}^3}$, μ_c= 0.3

Aluminum : E_m= 70 Gpa, $\rho_m = 2702\,\frac{\text{kg}}{\text{m}^3}$, μ_m= 0.3

Table 1 : Numerical calculations based on kinematic boundary conditions (BC).

BC	x = -L/2	x = +L/2
SS	u=0, w=0	w=0
CC	u=0, w=0, ϕ=0, w'=0	u=0,w=0, ϕ=0, w'=0

The characteristics of the TDFGTB material fluctuate in axial (L) and thickness (h) directions, according to power-law distribution. The dimensionless frequency (λ) parameter is used to represent the results.

$$\lambda=\frac{\omega L^2}{h}\sqrt{\frac{\rho_m}{E_m}} \quad (39)$$

4.1. Validation

The selection of taper ratios, aspect ratios, and gradation exponents for beam analysis involves a balance between structural requirements, geometric constraints, numerical considerations, and the objectives of the study. These parameters play a crucial role in defining the geometry and behavior of the beams under investigation and are chosen thoughtfully to ensure the relevance and

reliability of the analysis. For the numerical analysis, it is assumed that the material properties of the beam are homogeneous throughout, the material behaviour is linear and the load is distributed uniformly to facilitate the present investigation. A thorough and meticulous validation of the TDFGTB using RHSDT is performed using the nondimensional frequency as equation (39). Table 2 displays the results and comparisons based on idealized beams with various BCs. The current study's findings slightly deviate from those published by Shanab et al. [16]. For the CC beam, the frequency results in Table 3 are also the same; the deviation is attributed to the fact that the present study deals with the RHSDT, in which the shear stress is made zero at the top and bottom surfaces of the beam for accuracy result, whereas Shanab et al. [16] theory was related to the TBT, in which the shear shape function and the shear factor couldn't be considered.

Table 2 : Comparison of frequency values of SS TDFGTB based on taper ratio (n=0.0), and gradation exponents (p) at L/h = 5

Theory	P=0	P=0.5	P=1	P=2	P=5	P=10
TBT [16]	10.5	14.4	15.7	16.7	17.3	17.5
RHSDT	11.4	15.5	16.5	17.5	18.3	18.3
% Error	7.1%	6.8%	4.9%	4.6%	5.3%	5.4%

Table 3 : Comparison of frequency values of SS 2D-FGTB based on different taper ratio (n=0.5), and gradation exponents (p) at L/h = 5

Theory	P=0	P=0.5	P=1	P=2	P=5	P=10
TBT [16]	12.8	17.7	19.3	20.5	21.2	21.3
RHSDT	13.9	18.8	20.4	21.5	22.2	22.3
% Error	7.1%	5.5%	5.0%	4.8%	4.6%	4.6%

Table 2 compares the frequency results of RHSDT and TBT for SS beams, determined by the gradation exponent. RHSDT exhibits a higher frequency than TBT due to the implementation of the shear correction factor. We found a higher error percentage when comparing the results of the present study with [16]. The large difference in error is because [16] used TBT in the displacement direction only, without utilizing the shear correction factor. Rather, in the present study, a shear correction factor is considered in the refined shear deformation theory to fulfill the zero-shear stress on the top and bottom surfaces of the beam. Table 3 displays the comparison of the frequency results obtained from RHSDT and TBT for an SS beam with respect to the taper ratio. As the taper increases, it is observed that the frequency rises as well, which is influenced by the changing geometry.

Table 4 : Frequency values of SS TDFGTB based on different taper ratio (n = 0.0 and 0.5), aspect ratio (L/h=5)

n	pz	Px					
		0	0.5	1	2	5	10
0.0	0	11.4	13.5	14.8	16.3	17.7	18.1
	0.5	13.8	15.5	16.3	17.3	18.0	18.3
	1	14.6	15.8	16.5	17.3	18.119	18.3
	2	15.4	16.4	16.9	17.5	18.2	18.3
	5	16.4	17.0	17.4	17.8	18.3	18.4
	10	17.1	17.5	17.7	18.0	18.4	18.5
0.5	0	13.9	16.8	18.4	20.2	21.8	22.2
	0.5	16.8	18.8	19.9	21.0	22.0	22.3
	1	17.8	19.5	20.4	21.3	22.1	22.3
	2	18.8	20.1	20.8	21.5	22.2	22.3
	5	20.1	20.9	21.3	21.8	22.2	22.3
	10	20.9	21.4	21.7	22.0	22.3	22.3

Table 5 : Comparision of frequency values of CC TDFGTB based on different taper ratio (n=0.1 & 0.5) at aspect ratio (L/h=5).

Theory	P=0	P=0.5	P=1	P=2	P=5	P=10
RHSDT at n = 0.0	17.8	21.6	22.9	23.9	24.6	24.7
RHSDT at n = 0.5	19.4	24.2	25.8	27.0	27.7	27.8

Table 6 : Frequency values of SS TDFGTB based on different taper ratio (n=0.0, 0.5), aspect ratio (L/h=5).

n	Pz	Px					
		0	0.5	1	2	5	10
0.0	0	17.8	19.9	21.2	22.6	24.1	24.5
	0.5	20.2	21.6	22.5	23.4	24.3	24.6
	1	21.0	22.2	22.9	23.7	24.4	24.6
	2	21.8	22.8	23.3	23.9	24.5	24.6
	5	22.8	23.4	23.8	24.2	24.6	24.7
	10	23.5	23.9	24.1	24.4	24.6	24.7

0.5	0	19.4	22.2	23.9	25.6	27.2	27.6
	0.5	22.3	24.2	25.3	26.5	27.5	27.7
	1	23.3	24.9	25.8	26.7	27.5	27.7
	2	24.3	25.6	26.3	27.0	27.6	27.8
	5	25.5	26.3	26.8	27.3	27.7	27.8
	10	26.4	26.9	27.2	27.5	27.7	27.8

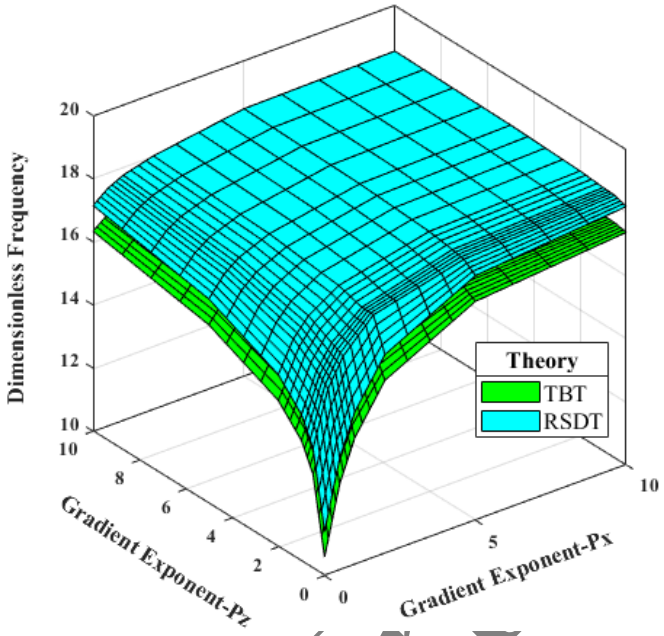

Fig 3 : Frequency values of SS TDFGTB at aspect ratio (L/h=5), taper ratio (n=0.0)

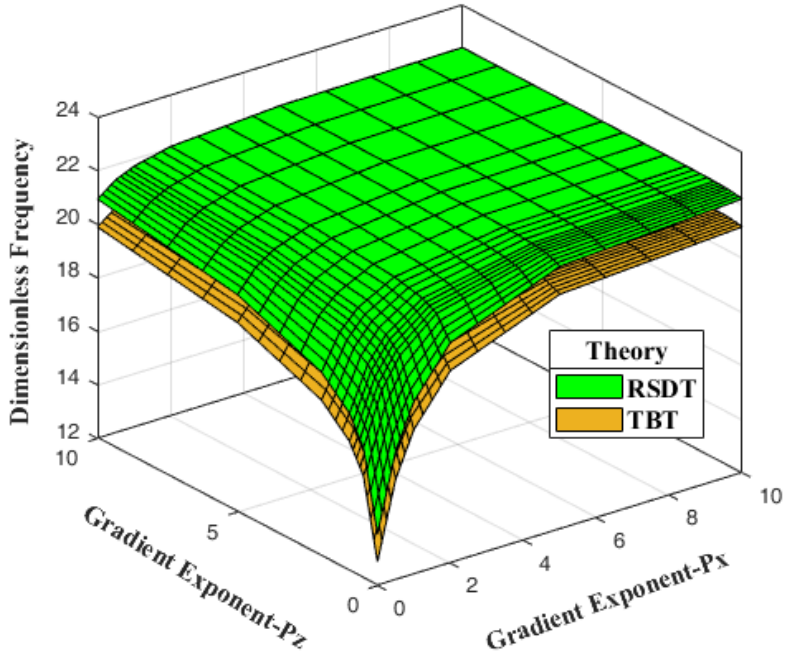

Fig 4 : Frequency values of SS TDFGTB at aspect ratio (L/h=5), taper ratio (n=0.5)

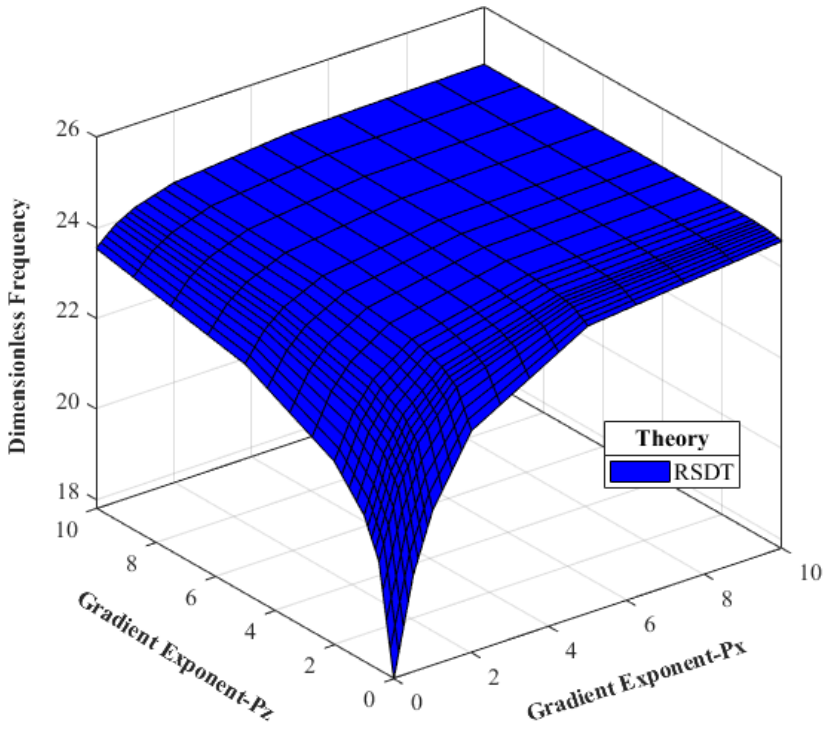

Fig 5 : Frequency values of CC TDFGTB at aspect ratios (L/h= 5), taper ratio (n=0.0)

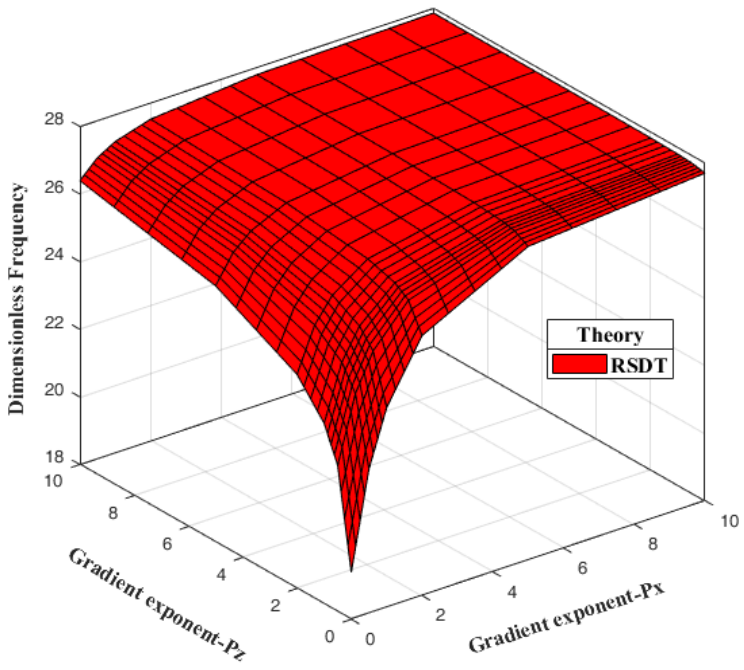

Fig 6: Frequency values of CC TDFGTB at aspect ratios (L/h= 20), taper ratio (n=0.5)

Under SS boundary conditions, the suggested theory is applied to assess and compare the results of free vibration with those anticipated by a taper nanobeam [16]. Satisfactory results are predicted by the presented theory. The remaining numbers, as shown in Table 5, are likewise appropriate for CC. Since the beam width is constant in this case, the applied load is constant along the length of the beam, but "moment of inertia" and "elastic modulus" vary with the beam length. The effects of the non-uniform parameter on the thickness variation, h(x), as well as the maximum dimensionless vibration at different power-law exponents and supporting types are discussed. The variation in the moment of inertia is caused by the change in thickness that takes place throughout the length of the beam. Table 4 and Table 6 show that the dimensionless frequency would rise for all types of supporting structures. Fig 3 and Fig 4 show that for SS beams and Fig 5 and Fig 6 show that the non-uniformity parameter reduces with *n*, however, the increase is dependent on the types of supporting elements.

Fig. 3 indicates the frequency differences between the TBT and the RHSDT for the SS beam at zero taper. The frequency increases with an increase in the gradient indexes in the *x* and *z* directions because the beam is transformed from metal to ceramic. In ceramic, the young modulus is higher than in metal, so the ceramic is stiffer and tends to vibrate at higher frequencies. Fig. 4 indicates the frequency differences between the TBT and RHSDT for the SS beam at 0.5 taper. The frequency increases with an

increase in the gradient indexes in the *x* and *z* directions because the beam convert from metal to ceramic. In ceramic, the young modulus is higher than in metal so the ceramic is stiffer and tends to vibrate at higher frequencies. Fig. 5 indicates the frequency at RHSDT for the CC beam at zero taper. The frequency increases with an increase in the gradient indexes in the *x* and *z* directions because the beam convert from metal to ceramic. In ceramic, the young modulus is higher than in metal, so the ceramic is stiffer and tends to vibrate at higher frequencies. Fig. 6 indicates the frequency at RHSDT for the CC beam at 0.5 taper ratio. The frequency increases with an increase in the gradient indexes in the *x* and *z* directions because the beam convert from metal to ceramic. In ceramic, the young modulus is higher than in metal, so the ceramic is stiffer and tends to vibrate at higher frequencies. As Table 4, the SS beam shows the highest rate of dimensionless frequency when compared to other supports such as CC. The placement of the clamped end, the distribution of young modulus, and the change in the moment of inertia were the key factors that affected the maximum dimensionless frequency and its rate of change. The taper ratio of a TDFGTB can lead to changes in the distribution of mass and stiffness along the length of the beam. This alteration can affect the natural frequencies of vibration modes. Higher taper ratios generally result in higher frequency responses due to the concentration of mass/stiffness towards one end of the beam. The aspect ratio (length-to-width ratio) of the beam can influence its bending behavior. For slender beams (high aspect ratios), higher frequency responses are typically observed due to the dominance of bending deformation modes. However, extremely high aspect ratios might introduce buckling instability, which can affect the frequency responses differently.

In contrast to the effects of thickness variation and the combination of thickness variation and width variation, where it has the greatest effects, the effects of width variation on the vibration in the beam are often not significant. Reducing the non-uniformity parameters implies that variances are causing the dimensionless vibration to rise. An SS beam experiences a rise in dimensionless vibration in addition to a change in the maximum dimensionless vibration's position due to the impacts of width variation, thickness variation, and both width and thickness variation. Variations in thickness as well as width contribute to an increase in dimensionless vibration. In most situations, the mid-span of an SS beam corresponds to the point of maximum vibration (i.e., x = l/2). It appears that both variations in the elastic modulus distribution and variations in the beam size cause the position of the dimensionless vibration to vary.

The introduction of a RHSDT for studying the vibration behavior of TDFGTB resulted in the presence of computational complexity. The incorporation of higher-order elements required a more complex formulation and technique for finding a solution. In order to tackle this difficulty, rigorous validation and verification procedures were carried out to guarantee the precision of the numerical implementation. Ensuring the satisfaction of boundary conditions posed challenges, particularly in formulating admissible functions to meet the prescribed constraints. The incorporation of Ritz-type solutions using algebraic polynomials facilitated the fulfillment of boundary conditions in both directions, while convergence studies were conducted to validate the chosen boundary conditions and ensure their consistency with physical principles.

5. Conclusions

This work uses a variational formulation based on RHSDT to construct a TDFGTB model. Constructed equations and related border conditions that take vibration and the neutral axis into account while applying the Hamilton principle concurrently. This is achieved by applying the two concepts at the same time. Apart from the properties of the material, the model is composed of surface elasticity constants and a material length scale parameter that change along the length and thickness directions of the beam according to the power law. The TDFGTB model was developed using Ritz solutions, which yielded an analytical solution for the vibration responses of SS and CC TDFGTB. Ritz Solutions looked into how different material and geometrical parameters affected the vibration responses using a thorough parametric analysis. The following is a summary of the main findings:

- The utilization of RHSDT captures the complexities of TDFGTBs' vibration behavior and also, by employing Lagrange equations and Ritz-type solutions, the study validates the applicability of RHSDT in modeling FGM structures, thereby contributing to the validation and refinement of analytical techniques for FGM analysis.
- The surface residual stress and the structure effect make the beam stiffer, which raises the anticipated vibration.
- The stiffness-hardening of the beam is increased by raising the gradient exponents in its thickness (P_z) and/or length (P_x), which consequently increases its vibration. This is attributed to the variations in the material properties across the length and thickness of the beam. Furthermore, higher gradient index implies steeper variation leading to more significant changes in the stiffness.
- The vibration of the taper beam is increased in proportion to the material's aspect ratio due to its stiffness-hardening effect. A higher aspect ratio typically corresponds to a longer and potentially narrower beam, which may exhibit greater stiffness-hardening due to variations in material properties. Consequently, the beam becomes less flexible and more resistant to deformation, leading to increased vibration under applied loads.
- As the taper ratio decreases, the TDFGTB vibrates more, suggesting that the beam may eventually fracture.
- The results serve as a benchmark for assessing the accuracy and reliability of existing beam theories in predicting the vibration behavior of TDFGTBs. This helps validate the efficacy of different analytical approaches and identifies areas for improvement in existing beam theories.

Applications: In the field of structural engineering and design, understanding the frequency responses of bi-directional functionally graded taper beams is crucial. This information can be used to improve the design of buildings, bridges, and aerospace components to obtain better performance under varying loads, as well as other industries where high-performance and lightweight materials are essential. The beam's edges are assumed by RHSDT to be either clamped or merely supported. But in reality, a beam might have more intricate boundary conditions, such partially or freely clamped edges, which could compromise the accuracy of the study.

References

[1] G. P. Sinha, B. Kumar, Review on vibration analysis of functionally graded material structural components with cracks, *Journal of Vibration Engineering & Technologies,* Vol. 9, pp. 23-49, 2021.

[2] P. Bridjesh, N. K. Geetha, B. Yelamasetti, Numerical investigation on buckling of two-directional porous functionally graded beam using higher order shear deformation theory, *International Journal on Interactive Design and Manufacturing (IJIDeM)*, pp. 1-14, 2023.

[3] V. Burlayenko, R. Kouhia, S. Dimitrova, One-dimensional vs. three-dimensional models in free vibration analysis of axially functionally graded beams with non-uniform cross-sections, *Mechanics of Composite Materials*, pp. 1-20, 2024.

[4] G. Reddy, P. Bridjesh, B. Reddy, K. Reddy, Comparison of Deflection in Two-Directional Functionally Graded Tapered Beam, *Mechanics of Advanced Composite Structures,* Vol. 11, No. 1, pp. 191-202, 2024.

[5] Y. Liang, S. Zheng, H. Wang, D. Chen, Nonlinear isogeometric analysis of axially functionally graded graphene platelet-reinforced composite curved beams, *Composite Structures,* Vol. 330, pp. 117871, 2024.

[6] R. Nazemnezhad, A semi analytical nonlinear approach for Size-dependent analysis of longitudinal vibration in terms of axially functionally graded nanorods, *Mechanics of Advanced Composite Structures*, 2024.

[7] H. Pekel, E. Erdurcan, Determination of natural frequencies of non-uniform aluminum beams coated with functionally graded material, *Materialwissenschaft und Werkstofftechnik,* Vol. 55, No. 2, pp. 204-215, 2024.

[8] R. Moalefshahri, Nonlinear vibrations of a cantilevered conical beam with axially functionally graded material carrying a longitudinally loaded mass, *Mechanics Based Design of Structures and Machines*, pp. 1-11, 2024.

[9] Z. Lakhdar, S. M. Chorfi, S. A. Belalia, K. M. Khedher, A. E. Alluqmani, A. Tounsi, M. Yaylacı, Free vibration and bending analysis of porous bi-directional FGM sandwich shell using a TSDT p-version finite element method, *Acta Mechanica*, pp. 1-30, 2024.

[10] Ş. D. Akbaş, Material Nonlinear Static Analysis of Axially Functionally Graded Porous Bar Elements, *Journal of Computational Applied Mechanics*, 2024.

[11] K. Hosseini-Hashemi, R. Talebitooti, S. Hosseini-Hashemi, R. Nazemnezhad, A unique and comprehensive approach to investigate the transverse free vibration of non-uniform and functionally graded Euler–Bernoulli beams, *Journal of the Brazilian Society of Mechanical Sciences and Engineering,* Vol. 45, No. 10, pp. 551, 2023.

[12] M. Mohammadi, M. Goodarzi, M. Ghayour, A. Farajpour, Influence of in-plane pre-load on the vibration frequency of circular graphene sheet via nonlocal continuum theory, *Composites Part B: Engineering,* Vol. 51, pp. 121-129, 2013.

[13] P. Elyasi, B. N. Neya, A. R. Firoozjaee, Free vibration of viscoelastic nonlocally damped tapered axially functionally graded beams using the state-space formulation, *Engineering Structures,* Vol. 288, pp. 116183, 2023.

[14] E. Demirkan, M. Çelik, R. Artan, Slope Deflection Method in Nonlocal Axially Functionally Graded Tapered Beams, *Applied Sciences,* Vol. 13, No. 8, pp. 4814, 2023.

[15] V. Kumar, S. Singh, V. Saran, S. Harsha, Vibration response analysis of tapered porous FGM plate resting on elastic foundation, *International Journal of Structural Stability and Dynamics,* Vol. 23, No. 02, pp. 2350024, 2023.

[16] M. Mohammadi, M. Hosseini, M. Shishesaz, A. Hadi, A. Rastgoo, Primary and secondary resonance analysis of porous functionally graded nanobeam resting on a nonlinear foundation subjected to mechanical and electrical loads, *European Journal of Mechanics-A/Solids,* Vol. 77, pp. 103793, 2019.

[17] T. A. Aslan, A. R. Noori, B. Temel, An efficient approach for free vibration analysis of functionally graded sandwich beams of variable cross-section, in *Proceeding of,* Elsevier, pp. 105397.

[18] R. A. Shanab, M. A. Attia, On bending, buckling and free vibration analysis of 2D-FG tapered Timoshenko nanobeams based on modified couple stress and surface energy theories, *Waves in Random and Complex Media,* Vol. 33, No. 3, pp. 590-636, 2023.

[19] B. Gupta, P. Sharma, S. Rathore, Free vibration analysis of AFGPM non-uniform beam: A mathematical modeling, *Journal of Vibration Engineering & Technologies,* Vol. 11, No. 7, pp. 2945-2954, 2023.

[20] S. Mirzaei, M. Hejazi, R. Ansari, Isogeometric analysis of small-scale effects on the vibration of functionally graded porous curved microbeams based on the modified strain gradient elasticity theory, *Acta Mechanica,* Vol. 234, No. 10, pp. 4535-4557, 2023.

[21] M. Mohammadnejad, Free vibration analysis of axially functionally graded beams using Fredholm integral equations, *Archive of Applied Mechanics,* Vol. 93, No. 3, pp. 961-976, 2023.

[22] D. Liu, J. Su, L. Zhao, X. Shen, State-Space Formulation for Buckling and Free Vibration of Axially Functionally Graded Graphene Reinforced Nanocomposite Microbeam under Axially Varying Loads, *Materials,* Vol. 17, No. 6, pp. 1296, 2024.

[23] K. Yee, O. Z. S. Ong, M. H. Ghayesh, M. Amabili, Various homogenisation schemes for vibration characteristics of axially FG core multilayered microbeams with metal foam face layers based on third order shear deformation theory, *Applied Mathematical Modelling,* Vol. 125, pp. 189-217, 2024.

[24] M. Mohammadi, A. Farajpour, A. Moradi, M. Ghayour, Shear buckling of orthotropic rectangular graphene sheet embedded in an elastic medium in thermal environment, *Composites Part B: Engineering,* Vol. 56, pp. 629-637, 2014.

[25] F. Bargozini, M. Mohammadimehr, The theoretical and experimental buckling analysis of a nanocomposite beams reinforced by nanorods made of recycled materials, *Polymer Composites,* Vol. 45, No. 4, pp. 3327-3342, 2024.

[26] F. Bargozini, M. Mohammadimehr, E. A. Dawi, M. Salavati-Niasari, Buckling of a sandwich beam with carbon nano rod reinforced composite and porous core under axially variable forces by considering general strain, *Results in Engineering*, pp. 101945, 2024.

[27] A. A. Monajemi, M. Mohammadimehr, Stability analysis of a spinning soft-core sandwich beam with CNTs reinforced metal matrix nanocomposite skins subjected to residual stress, *Mechanics Based Design of Structures and Machines,* Vol. 52, No. 1, pp. 338-358, 2024.

[28] M. Mohammadi, A. Farajpour, A. Moradi, M. Hosseini, Vibration analysis of the rotating multilayer piezoelectric Timoshenko nanobeam, *Engineering Analysis with Boundary Elements,* Vol. 145, pp. 117-131, 2022.

[29] A. Amiri, M. Mohammadimehr, M. I. Rahaghi, Vibration analysis of a micro-cylindrical sandwich panel with reinforced shape-memory alloys face sheets and porous core, *The European Physical Journal Plus,* Vol. 136, No. 8, pp. 887, 2021.

[30] M. Charekhli-Inanllo, M. Mohammadimehr, The effect of various shape core materials by FDM on low velocity impact behavior of a sandwich composite plate, *Engineering Structures,* Vol. 294, pp. 116721, 2023.

[31] A. Farazin, M. Mohammadimehr, H. Naeimi, F. Bargozini, Design, fabrication, and evaluation of green mesoporous hollow magnetic spheres with antibacterial activity, *Materials Science and Engineering: B,* Vol. 299, pp. 116973, 2024.

[32] A. Farazin, M. Mohammadimehr, H. Naeimi, Flexible self-healing nanocomposite based gelatin/tannic acid/acrylic acid reinforced with zinc oxide nanoparticles and hollow silver nanoparticles based on porous silica for rapid wound healing, *International Journal of Biological Macromolecules,* Vol. 241, pp. 124572, 2023.
[33] F. Bargozini, M. Mohammadimehr, E. A. Dawi, R. Monsef, Z. Heydariyan, M. Salavati-Niasari, Development and performance analysis of a 316 stainless steel autoclave for facile fabrication of carbon nanoarchitectures derived from natural potato and starch, *Journal of Materials Research and Technology,* Vol. 23, pp. 3126-3136, 2023.
[34] K. Alambeigi, M. Mohammadimehr, M. Bamdad, T. Rabczuk, Free and forced vibration analysis of a sandwich beam considering porous core and SMA hybrid composite face layers on Vlasov's foundation, *Acta Mechanica,* Vol. 231, pp. 3199-3218, 2020.
[35] M. K. Mogehi, M. Mohammadimehr, N. D. Duc, Vibration analysis of a sandwich Timoshenko beam reinforced by GOAM/CNT with various boundary conditions using VIM, *Materials Science and Engineering: B,* Vol. 304, pp. 117364, 2024.
[36] M. Arabzadeh-Ziari, M. Mohammadimehr, E. Arabzadeh-Ziari, M. Asgari, Deflection, buckling and vibration analyses for a sandwich nanocomposite structure with foam core reinforced with GPLs and SMAs based on TSDBT, *Journal of Computational Applied Mechanics,* Vol. 55, No. 2, pp. 289-321, 2024.
[37] M. Mohammadi, A. Farajpour, A. Rastgoo, Coriolis effects on the thermo-mechanical vibration analysis of the rotating multilayer piezoelectric nanobeam, *Acta Mechanica,* Vol. 234, No. 2, pp. 751-774, 2023.